Journal of Sound and Vibration 330 (2011) 603–614

Contents lists available at ScienceDirect

Journal of Sound and Vibration

journal homepage: www.elsevier.com/locate/jsvi

Dynamic analysis and optimal design of a passive and an active piezo-electrical dynamic vibration absorber

Sang-Myeong Kim [a,*], Semyung Wang [a], Michael J. Brennan [b]

[a] Mechatronics, Gwangju Institute of Science and Technology, 261 Cheomdan-gwagiro, Buk-gu, Gwangju 500-712, Republic of Korea
[b] Institute of Sound and Vibration Research, University of Southampton, University Road, Highfield, Southampton SO17 1BJ, United Kingdom

ARTICLE INFO

Article history:
Received 30 March 2010
Received in revised form
3 August 2010
Accepted 5 September 2010
Handling Editor: L.G. Tham
Available online 12 October 2010

ABSTRACT

This paper is concerned with the dynamic analysis and parameter optimization of both passive and active piezo-electrical dynamic vibration absorbers that are strongly coupled with a single degree of freedom vibrating structure. The passive absorber is implemented by using an $R_s \| L_s$ parallel shunt circuit while the active absorber is implemented by feeding back the acceleration of the structure through a second-order lowpass filter. An impedance-mobility approach is used for the electromechanical coupling analysis of both types of absorbers coupled with the structure. Using this approach it is demonstrated that the passive and active absorbers can be made exactly equivalent. A maximally flat frequency response strategy is used to find the optimal damping ratio of the passive absorber while a robust, optimal control theory is used to find that for the active absorber. It is found that the passive optimization strategy corresponds to an optimal, robust feedback control of 2 dB spillover. Simulations and experiments are conducted to support the theoretical findings.

© 2010 Elsevier Ltd. All rights reserved.

1. Introduction

Piezoelectric materials, such as PZT ceramics, are widely used to suppress vibrations in many actively controlled engineering structures. One of the reasons for this is because they are relatively easy to install. When they are embedded in a structure they are electromechanically coupled with the structure due to the piezoelectric effects producing an electrical field (i.e., charge) in response to a mechanical stress and vice versa. A passive or active electrical network is usually connected to the two electrodes of such a piezoceramic material to suppress structural vibration. By using a shunt resistor with the piezoceramic element, for example, electrical damping is imposed on the structure. Adding an inductor means that there is an electrical resonance circuit because of the inherent capacitance of the piezoceramic element, which can then be strongly coupled to a particular vibration mode of concern [1–3]. The vibration suppression mechanism in this resonant shunt damping has been thought to be similar to that of the mechanical dynamic vibration absorber [1]. Such a dynamic absorber effect can also be realized actively by feeding back the acceleration of the structure through a second-order lowpass filter [4]. Here, the resonant shunt circuit is referred to as a passive *electrical dynamic absorber* (EDA) while the active control circuit is referred to as an active EDA. In this paper, single degree-of-freedom passive and active EDAs are considered as in the Refs. [1–3]. Unlike the work reported in these publications, however, here an impedance-mobility approach [5] is used to analyze the dynamics of both types of EDA, each of which is then designed separately using optimization strategies for passive [3] and active [4] systems to finally reveal the relationship between the two strategies.

* Corresponding author. Tel.: +82 10 4923 0113; fax: +82 62 715 2384.
E-mail addresses: smkim123@hanmail.net (S.-M. Kim), smwang@gist.ac.kr (S. Wang), mjb@isvr.soton.ac.uk (M.J. Brennan).

0022-460X/$ - see front matter © 2010 Elsevier Ltd. All rights reserved.
doi:10.1016/j.jsv.2010.09.004

The results obtained from these unified approaches employed for analysis and design (or control) are reported in this paper.

The coupling between structures and passive piezo-electrical networks has been treated extensively in the literature in applications where shunt resonant control has been used, for example, [1–3], and energy harvesting [6,7]. Regardless of whether a passive or active EDA is considered, the approach in this paper treats it as a subsystem characterized by an impedance and combines this impedance with that of the host structure. Thus, the coupling can be analyzed in a conventional easy way using the mass ratio between the host structure and the absorber. A single degree-of-freedom (SDOF) host structure is considered throughout the paper for simplicity. For resonant shunt damping, a parallel $R_s\|L_s$ circuit consisting of a shunt resistor and a shunt inductor is used. Using this approach it is shown that the passive and active absorbers can be made exactly equivalent.

Various optimization strategies are available to find the optimal absorber damping [2,3] of the $R_s\|L_s$ parallel shunt circuit. Here, the focus is on the maximally flat frequency response strategy [3], which is to yield the broadest half-power bandwidth in the mobility response of the coupled structure. An analytical solution is newly derived for the optimal absorber damping by using conventional mechanical systems analysis, which is then re-examined from the perspective of robust feedback control theory to expose the relationship between the two methods. Consequently it is straightforward to determine the optimal parameters for an active EDA. Experimental results are presented to support the theoretical findings for analysis and control. There is also an Appendix to this paper, which discusses the sign conventions used for the piezoelectric coupling formulation.

2. Impedance-mobility approach

2.1. Electromechanical coupling formulation

Consider the SDOF structural vibration system (mass m_s, spring k_s, and damper c_s) embedded with a piezoceramic material of capacitance C_p shown in Fig. 1. Two types of vibration control are considered: a passive technique using a shunt load impedance Z_L as shown in Fig. 1(a) and an active technique feeding back the structural motion to the piezoceramic actuator (represented as a force actuator F_A) via a control filter $-H(j\omega)$ as shown in Fig. 1(b), where the minus sign indicates negative feedback. The voltage V across the piezoceramic element is also shown together with the poling direction, which are required for a consistent mathematical formulation as what follows. In this paper, the general assumptions and sign conventions in the IEEE standard on piezoelectricity [8] are closely followed with the exception of the sign convention for the piezoelectric constant d_{ij}. Here, this is defined to be always positive, as is often done in the literature [6,7]. As there is a different sign convention in common use, for example, [3], these two conventions are compared and the consequences are discussed in the Appendix. Hereafter, the mechanical system is referred to as the '*structure*' while the passive or active circuit is referred to as the '*absorber*.'

The dynamic equation of the structure subject to an external excitation force F is given by

$$Z_S v = F - F_A, \tag{1}$$

where v is velocity with respect to the ground, $Z_S = j\omega m_s + c_s + (k_s + k_p)/j\omega$ is the structural impedance which includes the mechanical stiffness k_p of the piezoceramic element (measured in its short-circuit state), $j = \sqrt{-1}$, the effective force acting on the structure is $F_S = F - F_A$ and ω is the angular frequency. The force $F_A = \phi V$ is the electrically induced force due to piezoelectricity that resists the motion, and ϕ (which is always *positive*—see the Appendix) is the *electromechanical* (*EM*) *conversion* or *coupling factor* of the piezoceramic element and has the unit of (N/V). The dynamic equation of the absorber

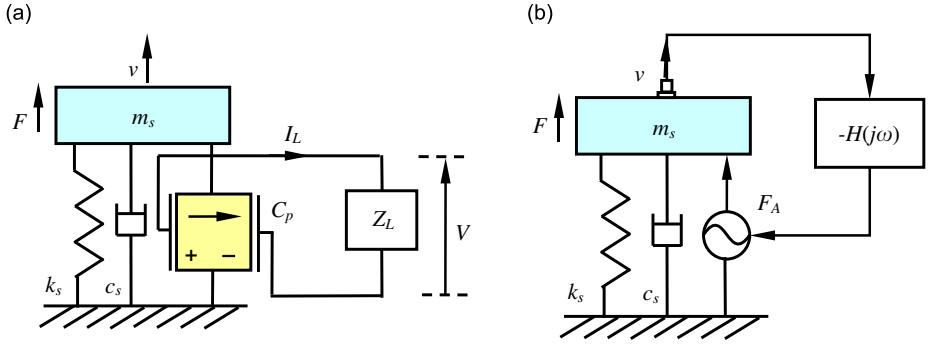

Fig. 1. Passive and active control treatments, the shunt circuit Z_L and the control filter $-H(\omega)$, to a single degree of freedom vibration system embedded with a piezoceramic actuator of capacitance C_p. The arrow inside the piezoceramic indicates the poling direction: (a) passive control and (b) active control.

subject to excitation v can be written as

$$Z_A^{-1}V = \phi v, \tag{2}$$

where $Z_A = (Z_p^{-1} + Z_L^{-1})^{-1}$ is the impedance of the absorber, V is voltage as indicated in Fig. 1(a), $Z_p = (j\omega C_p)^{-1}$ is the electrical impedance of the piezoceramic with C_p being the capacitance, and $Z_L = V/I_L$ is the shunt load impedance with current I_L. The excitation term ϕv acts as a current source to the piezoceramic C_p and the load element Z_L. The factor ϕ now indicates the relationship between a motion and the electric current or charge developed and has the unit of (A/m s^{-1}) or (C/m), respectively. Eq. (1) is related to the actuator equation while Eq. (2) to the sensor equation of a piezoelectric material [8].

Combining Eqs. (1) and (2) yields

$$\begin{bmatrix} Z_S & \phi \\ -\phi & Z_A^{-1} \end{bmatrix} \begin{Bmatrix} v \\ V \end{Bmatrix} = \begin{Bmatrix} F \\ 0 \end{Bmatrix}, \tag{3}$$

from which the familiar solution form of the impedance-mobility approach [5] is obtained as

$$v = \frac{Y_S}{1 + Y_S Z_{CA}} F, \tag{4}$$

where the structural mobility is $Y_S = Z_S^{-1}$ and the mechanically coupled absorber impedance is $Z_{CA} = \phi^2 Z_A$. The strength of coupling between the structure and the absorber is governed by the term $|Y_S Z_{CA}|$ in the denominator [5], where $|\bullet|$ denotes the absolute value. This term is examined further, later in this section with a specific model of the absorber. From a negative feedback control perspective, Eq. (4) can be rewritten as

$$v = \frac{G(j\omega)}{1 + G(j\omega)H(j\omega)} F, \tag{5}$$

in which $G(j\omega) = Y_S$ is the plant and $H(j\omega) = Z_{CA}$ is the controller. Eq. (4) is a view of the system from the impedance-mobility approach while Eq. (5) is a feedback control view. These two different views of the passive absorber are, respectively, illustrated in Fig. 2(a) and (b).

Now, consider the active control system in Fig. 1(b). Eq. (1) is then $Z_S v = F + F_A$ in which $F_A = -H(j\omega)v$ is now the active control force. Substituting F_A and $G(j\omega) = Y_S$ yields Eq. (5). Eq. (4) is also valid (in control terms, absolutely stable), as long as $H(j\omega)$ is of the same form as Z_{CA} in terms of number and locations of poles and zeros so as to have minimum phase characteristics [9]. Stability analysis for this case is *trivial* as the combined system is in theory completely passive. In practice, however, such unconditionally stable systems are realizable only approximately due to non-ideal operations of elements in the feedback loop including sensors, actuators, control filters and amplifiers [4,10].

2.2. Electrical and mechanical analogous models

Three shunt circuits are generally employed in the literature, which are illustrated in Fig. 3: (a) R_s shunt circuit using a resistor R_s, (b) $R_s - L_s$ series circuit using a resistor and an inductor L_s [1–3], and (c) $R_s \| L_s$ parallel circuit [2,3], where '$-$' denotes a series connection and '$\|$' is a parallel connection. The corresponding analogous mechanical models consisting of lumped mechanical elements (mass m_a, spring k_a, and damper c_a) are also shown in Fig. 3, where the velocity input v_E and the force F_E correspond to current I and voltage V, respectively, and the subscript E denotes an electrically induced variable. The conversion rules are given in Table 1. The electrical absorber impedances for the three cases are tabulated in Table 2 for reference. As the $R_s \| L_s$ circuit is most widely used, and because it has a similar performance to the $R_s - L_s$ circuit [3], it is considered for the remainder of this paper.

Connecting the electrically analogous model for the SDOF structure to the $R_s \| L_s$ circuit gives the complete analogous model shown in Fig. 4(a), where the structural mass, spring and damper are indicated by the analogous inductor, capacitor, and resistor, following the conversion rules in Table 1. An ideal transformer is used to match the dimensions between the

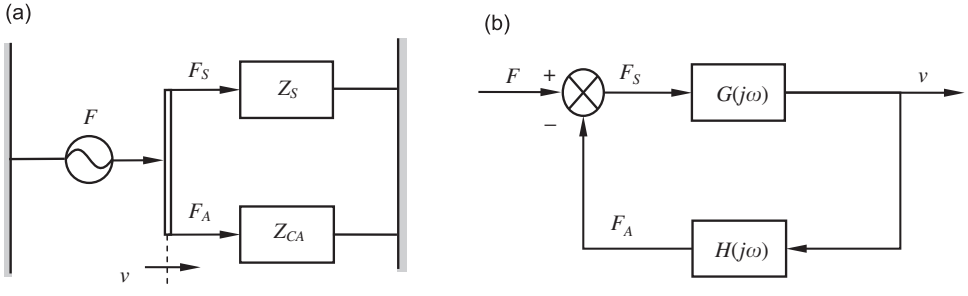

Fig. 2. Two different viewpoints to the passive and active control of the system in Fig. 1. The equality relations are $G(j\omega) = Y_S$ with $Y_S = Z_S^{-1}$ and $H(j\omega) = Z_{CA}$: (a) impedance-mobility view and (b) feedback control view.

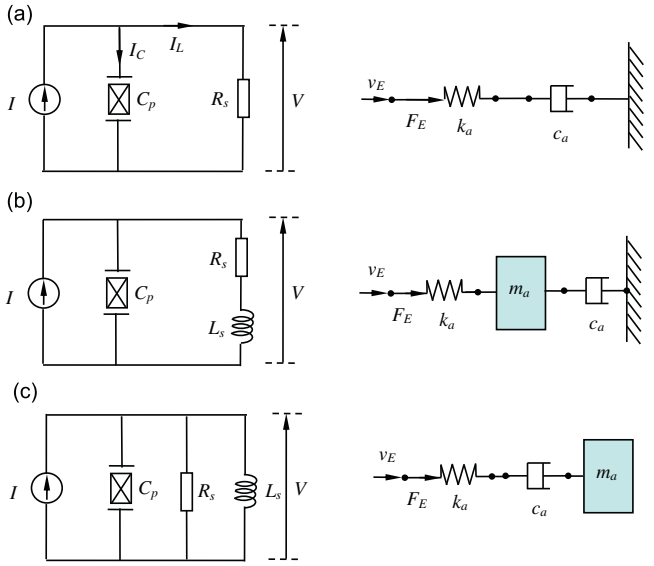

Fig. 3. Various shunt circuits and their analogous mechanical models: (a) R_s circuit, (b) R_s-L_s series circuit, and (c) $R_s\|L_s$ parallel circuit.

Table 1
Electro-mechanical conversion rules for the electrical dynamic absorbers in Fig. 3.

Elements	Spring	Mass	Damping	Force	Velocity
Electrical	C_p^{-1}	L_s	R_s	V	I
Mechanical	k_a	m_a	c_a	F_E	v_E
Coupled	$k_{ca}=\phi^2 k_a$	$m_{ca}=\phi^2 m_a$	$c_{ca}=\phi^2 c_a$	$F_A=\phi V$	$v=\phi^{-1} I$

Table 2
Impedances of the electrical dynamic absorber in Fig. 3.

Shunt circuit	Electrical impedance, $Z_A=V/I$	Mechanical impedance, $Z_A=F_E/v_E$
R_s	$Z_A^{-1}=j\omega C_p+R_s^{-1}$	$Z_A^{-1}=j\omega/k_a+c_a^{-1}$
R_s-L_s	$Z_A^{-1}=j\omega C_p+(R_s+j\omega L_s)^{-1}$	$Z_A^{-1}=(j\omega/k_a)+(c_a+j\omega m_a)^{-1}$
$R_s\|L_s$	$Z_A^{-1}=j\omega C_p+R_s^{-1}+(j\omega L_s)^{-1}$	$Z_A^{-1}=(j\omega/k_a)+c_a^{-1}+(j\omega m_a)^{-1}$

mechanical and electrical systems, which is given by

$$\begin{Bmatrix} F_A \\ v \end{Bmatrix} = \begin{bmatrix} \phi & 0 \\ 0 & \phi^{-1} \end{bmatrix} \begin{Bmatrix} V \\ I \end{Bmatrix}. \tag{6}$$

Some similar analogous models can be found for the R_s and R_s-L_s shunt circuits [1,11,12]. This electrical model can also be equivalently transformed into a mechanical one as shown in Fig. 4(b), where the new coupled terms (m_{ca}, k_{ca}, and c_{ca}) are introduced for the absorber and the relevant conversion rules are added to Table 1. Unlike the conventional two DOF system, it should be emphasized that the connection between spring and damper of the absorber is in series.

The structural mobility, which is the plant response $G(j\omega)$ in Fig. 2, can be written as

$$G(j\omega)=Y_S=\frac{1}{m_s}\,\frac{j\omega}{\omega_s^2-\omega^2+j2\varsigma_s\omega_s\omega}, \tag{7}$$

where the natural frequency is defined as $\omega_s=\sqrt{(k_s+k_p)/m_s}$, and the structural damping ratio can be obtained from $2\varsigma_s\omega_s=c_s/m_s$. From Table 2, the coupled absorber impedance of the $R_s\|L_s$ shunt circuit can be written as

$$Z_{CA}=\phi^2 k_a\,\frac{j\omega}{\omega_a^2-\omega^2+j2\varsigma_a\omega_a\omega}, \tag{8}$$

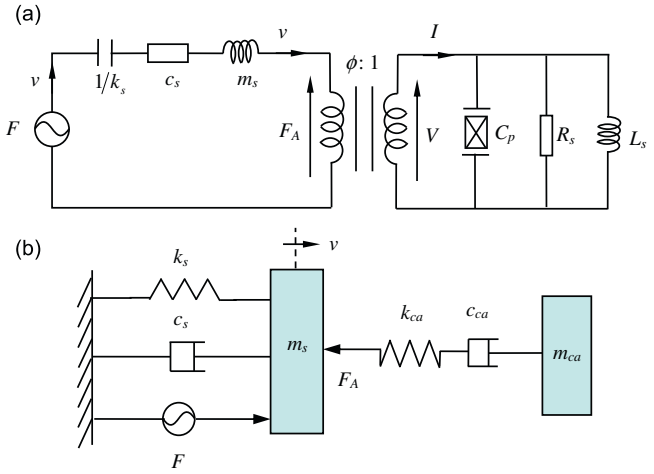

Fig. 4. Electrical (a) and mechanical (b) lumped-parameter analogous models of the electrical dynamic absorber using an $R_s\|L_s$ shunt circuit in Fig. 3(c). The conversion rules are given in Table 1.

where the natural frequency is defined as $\omega_a=\sqrt{1/(L_sC_p)}=\sqrt{k_a/m_a}$, and the damping ratio can be obtained from $2\varsigma_a\omega_a=1/(R_sC_p)=k_a/c_a$. For emphasis, the structural and absorber damping ratios in Eqs. (7) and (8) are rewritten as

$$\varsigma_s=\frac{c_s}{2\sqrt{m_sk_s}}, \tag{9a}$$

$$\varsigma_a=\frac{\sqrt{m_ak_a}}{2c_a}. \tag{9b}$$

It is important to note that the absorber damping ζ_a has been defined differently from the familiar form for the structure ζ_s. The two expressions in Eq. (9a, b) correspond to the two different damping ratio descriptions for the $R_s-C_s-L_s$ series and $R_s\|C_s\|L_s$ parallel circuits [13].

To be compatible with the passive absorber described in Eq. (8), the active control filter should be of the form:

$$H(j\omega)=h\omega_a^2\frac{j\omega}{\omega_a^2-\omega^2+j2\varsigma_a\omega_a\omega}, \tag{10}$$

where h is the gain of the control filter, and ω_a and ζ_a are the same as those defined for Eq. (8). Eq. (8) is substituted into Eq. (4) or Eq. (5) for passive control while Eq. (10) is substituted instead for active control. If the gain is set to be $h=\phi^2k_a/\omega_a^2$, Eqs. (8) and (10) are exactly equivalent. Thus the analogous models in Fig. 4 are valid for both passive and active EDAs.

2.3. Coupling strength analysis

The strength of coupling can be assessed by the term $|Y_SZ_{CA}|$, which is, in fact, the modulus of the open-loop frequency response function (FRF) $L(j\omega)=G(j\omega)H(j\omega)$ in feedback control terms. Combining Eqs. (7), (8) and introducing a dimensionless frequency $\Omega=\omega/\omega_n$ and the frequency tuning ratio $\alpha=\omega_s/\omega_a$ gives the open-loop FRF as

$$L(j\Omega)=-\sigma\Omega^2(1-\Omega^2+ja\Omega)^{-1}(1-\alpha^2\Omega^2+jb\alpha\Omega)^{-1}, \tag{11}$$

where $a=2\zeta_s$ and $b=2\zeta_a$ are the dimensionless half-power bandwidths of the structure and the absorber in Eqs. (7) and (8), normalized by ω_s and ω_a, respectively, The open-loop FRF is now described in terms of the *mass ratio* $\sigma=m_{ca}/m_s$, with m_{ca} being the coupled absorber mass for passive control. If the natural frequency of the absorber is exactly tuned to that of the structure (i.e., $\omega_a=\omega_s$), as a special case, this also represents the *stiffness ratio* $\sigma=k_{ca}/k_s$, with k_{ca} being the coupled absorber stiffness. The strength of coupling can now be judged by examining the mass ratio, which is frequency-independent and is more precisely written as

$$\sigma=\phi^2/(m_sC_p\omega_n^2)=\phi^2/(k_sC_p). \tag{12a}$$

The mass ratio σ, which has been interpreted as the generalized electromechanical coupling coefficient in the literature, is measurable from simple vibration tests with the piezoelectric element being in the open- and short-circuited conditions as given by [1,3]

$$\sigma=(\omega_{\text{open}}^2-\omega_s^2)/\omega_s^2, \tag{12b}$$

where the natural frequencies ω_{open} and ω_s correspond to the open and short electrical conditions, respectively. In the active EDA, the mass ratio is given by

$$\sigma = h/m_s \tag{12c}$$

and thus the gain of the filter in Eq. (10) is, in fact, the coupled absorber mass $h=m_{ca}$.

3. Parameter optimization

3.1. Active absorber

To assess the control performance, the velocity ratio $S(j\Omega)=v/v_0$ of the structure with (v) and without (v_0) control is used. This is, in fact, the sensitivity function S in feedback control terms. The velocity v_0 can be obtained by setting $V=0$ (e.g., short circuiting the piezoceramic) in Eq. (1). Since the sensitivity function is given by $S(j\Omega)=[1+L(j\Omega)]^{-1}$, the vibration reduction ratio (RR) is given in decibels by

$$RR(\text{dB}) = -20\log_{10}|1+L(j\Omega)|. \tag{13}$$

Following the robust control theory developed by Kim et al. [4], a control system is defined to be *stable* and *robust* with the degree of r if and only if the open-loop FRF locus $L(j\Omega)$ does not enclose or cross the circle of robustness of radius r centered at the instability point $(-1, 0)$, where $0<r<1$, that is

$$RR(\text{dB}) \le (-20\log_{10}r), \tag{14}$$

where the maximum level on the right of Eq. (14) can be interpreted as the allowable amount of vibration increase (i.e., maximum control spillover) after control. Thus the system can be optimized for the best performance within the limit of the given control spillover $RR_{(\max)} = (-20\log_{10}r)$.

In the optimization process, it is assumed that the natural frequency of the absorber is exactly tuned to that of the structure, i.e., $\omega_n=\omega_a=\omega_s$ [4], where ω_n indicates the tuned natural frequency. It is convenient to introduce a new variable $x=\Omega-\Omega^{-1}$ to further reduce Eq. (11) to a more manageable form for hand calculation as

$$L(jx) = \sigma(a+jx)^{-1}(b+jx)^{-1}. \tag{15}$$

For a real positive value of x, the corresponding roots of Ω are $\Omega_{2,1} = (\sqrt{x^2+4} \pm x)/2$, where $x=\Omega_2-\Omega_1$ because $\Omega_1=1/\Omega_2$, where $\Omega_2>1$. Thus the variable x is, in fact, a frequency bandwidth, which is bounded by $\Omega_1 \le x \le \Omega_2$. Note that the introduction of x transforms the fourth-order equation in Eq. (11) to the second-order form in Eq. (15). The normalized control bandwidth x_c, within which vibration reduction occurs, can be obtained from $|1+L(jx)|=1$, and is given by [4]

$$y_c = v+(\sigma/2), \tag{16}$$

in which $v=ab$, and $x_c = \sqrt{y_c}$. The simplified expression in Eq. (15) greatly facilitates solving the optimization problem with the robustness constraint given by Eq. (14). If the task is to find the optimal damping ratio $g=c_{ca}/c_s$ for a given bandwidth b under a prescribed robustness degree r, the exact solution is known and is given by [4]

$$g = ((\eta+1)(1-r^2)/r^2)\left(1+\sqrt{1-r^2((\eta-1)/(\eta+1))}\right), \tag{17}$$

where $\eta=\mu/v$ in which $\mu=(a^2+b^2)/2$. Since $\sigma=gab$, Eq. (17) can be rearranged by assuming that $a \ll b$ to give the optimal absorber damping ratio for a given mass ratio σ under a prescribed robustness degree r:

$$\varsigma_{a,\text{active}} \approx \sqrt{\frac{1-m}{2m^2}\sigma}, \tag{18}$$

where $m^2=1-r^2$.

3.2. Passive absorber

The optimization parameter with the $R_s \| L_s$ shunt circuit is the resistor R_s only, as the inductor is used for frequency tuning (i.e., $\omega_a=\omega_s$). In this paper, the so-called maximally flat FRF strategy [3], which yields the maximally flat FRF of the structural velocity with the absorber in place, is re-examined. An explicit analytical form for the optimal absorber damping ratio is newly determined. Let $Y_{CS}=v/F$ denote the coupled structural mobility response in Eq. (4) and write it in terms of the new variable x:

$$Y_{CS} = \frac{1}{c_s}\frac{a(b+jx)}{(a+jx)(b+jx)+\sigma}. \tag{19}$$

The condition to have the maximally flat FRF may be expressed mathematically as

$$|Y_{CS}(0)| = |Y_{CS}(jx_c)|, \tag{20}$$

which means that the velocity amplitude response at the uncoupled natural frequency when $x=0$ (equivalently, $\Omega=1$) is the same as those at the boundary frequencies (i.e., Ω_{c1} and Ω_{c2}) of the control bandwidth. Since $|Y_{CS}(jx_c)|=|Y_S(jx_c)|$ because of $|1+L(jx_c)|=1$ by definition, Eq. (19) can be rewritten as

$$|Y_{CS}(0)|=\frac{1}{c_s}\frac{ab}{ab+\sigma},\quad |Y_{CS}(jx_c)|=\frac{1}{c_s}\left|\frac{a}{a+jx_c}\right| \tag{21}$$

and applying Eq. (20) gives the exact explicit solution of the optimal damping ratio for the maximally flat FRF strategy, when $\omega_a=\omega_s$, as

$$\varsigma_{a,\text{passive}}=\sqrt{\sigma/2}. \tag{22}$$

The procedure employed here is, in essence, Den Hartog's fixed-point theory [14], but with an aim to achieve a maximally flat coupled mobility FRF response for a serially connected mass–spring–damper absorber. The maximum reduction (i.e., minimum reduction ratio) and the normalized control bandwidth can also be calculated. Combining Eqs. (13), (15) and (22) with $x=0$ gives

$$RR_{\text{passive(min)}}=-20\log_{10}\left(1+\sqrt{\sigma/(8\varsigma_s^2)}\right)\text{dB} \tag{23}$$

and combining Eqs. (16) and (22) gives

$$x_{c,\text{passive}}=\sqrt{(\sigma/2)+\varsigma_s\sqrt{8\sigma}}. \tag{24}$$

The control performance can be predicted from Eqs. (23) and (24) in which the terms σ and ζ_s can be easily identified by simple vibration tests. Eqs. (23) and (24) suggest that the EDA is effective for lightly damped structures. In other words, adding electrical damping may not be effective for highly damped structures unless the mass ratio σ can be made to be very large.

Finally, comparing Eqs. (18) and (22) reveals that the maximally flat FRF strategy corresponds to the optimal, robust control strategy with the robustness degree of $r=\sqrt{(\sqrt{5}-1)/2}$ or equivalently with the maximum spillover amount of

$$RR_{\text{passive(max)}}\approx 2\,\text{dB}, \tag{25}$$

provided that $\varsigma_s \ll \sqrt{\sigma/2}$. For a lightly damped structure with a moderate amount of absorber mass or spring, the maximally flat FRF strategy can thus be interpreted as the "*optimal, robust control of* 2 *dB spillover*" in feedback control parlance.

4. Experiments and simulations

For the experimental SDOF vibration system, a commercial piezoelectric inertial actuator (PCB Piezoelectronics 712A02) with a proof mass of 100 g was used; it was fixed in a heavy optical measurement table. Inside the actuator, piezoelectric materials are bonded to the upper and lower plates and generate a pulsating motion in response to the voltage input so as to vibrate the inertial mass [15]. Impact hammer tests (Endevco 2302-10) were conducted in four different cases as illustrated in Fig. 5. They are (1) when the input channel to the piezoelectric actuator was electrically shorted (i.e., the switch in Fig. 5 was connected to Terminal ①), (2) when the channel was electrically opened, (3) when the switch was connected to a shunt resonant circuit, and finally (4) when the switch was connected to an active control filter. In all cases, impacts were applied directly on the top surface of the accelerometer (B&K 4393) placed at the center of the cylindrical mass in order to avoid exciting non-symmetric modes of the circular-shaped actuator.

Fig. 6 shows the experimentally obtained velocity responses to 1 N force for the short- (dash-dot line) and open-circuit (dashed) conditions, which are tests (1) and (2) in Fig. 5, respectively. The simulation result (dotted) for each case is also overlaid using the parameters summarized in Table 3, where all the parameters were identified from the test results. The peak at around 1320 Hz is an inherent characteristic of the actuator itself. The most important parameter that can be identified from these tests is the mass ratio σ using Eq. (12b), and subsequently the EM conversion factor ϕ using Eq. (12a). They are also given in Table 3.

For test (3) with the passive EDA, an $R_s\|L_s$ shunt circuit was designed and the parameters were determined using the maximally flat FRF strategy. The optimal inductor of as high as about 3.9 H was synthesized by using Antoniou's gyrator circuit [3,16]. The gyrator circuit was built using two OP amps (Burr-Brown OPA445) with input supply voltages of ± 40 V [17], a capacitor, three cement resistors, and a variable resistor to set the effective inductance. All electrical components were chosen to withstand the high voltage from the piezoceramic actuator. Another variable resistor was used to set the resistance of the $R_s\|L_s$ shunt circuit to the optimal value of about 14.8 kΩ. The test velocity response (solid line) is compared with the original short-circuit plant response (dash-dot) in Fig. 7, where the responses are normalized by the maximum magnitude of the original response. The corresponding simulation result (dashed) is also overlaid for comparison. The simulation and experimental responses are quite flat within the control bandwidth as designed, and there is good agreement between them.

For the last test, the active EDA filter was designed by using the acceleration position feedback (APF) method as the acceleration signal was readily available from the accelerometer [4]. The control filter was implemented digitally in a target PC equipped with a DAQ board (NI PCI-6251), by using the Matlab ® xPC Target module. A signal conditioner (B&K

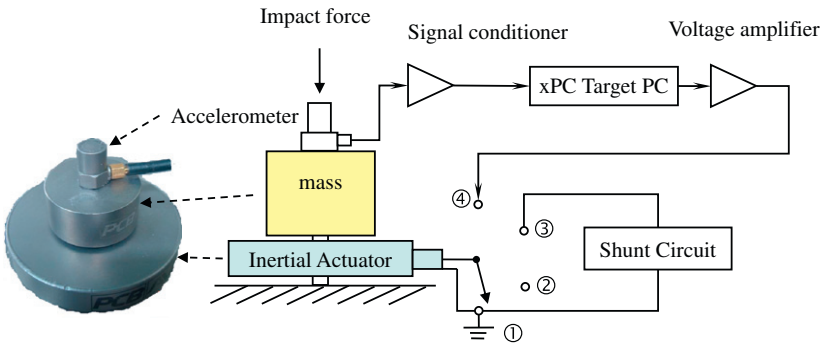

Fig. 5. Experimental setup for impact hammer tests in four different conditions: (1) short circuit, (2) open circuit, (3) passive EDA circuit, and (4) active EDA circuit.

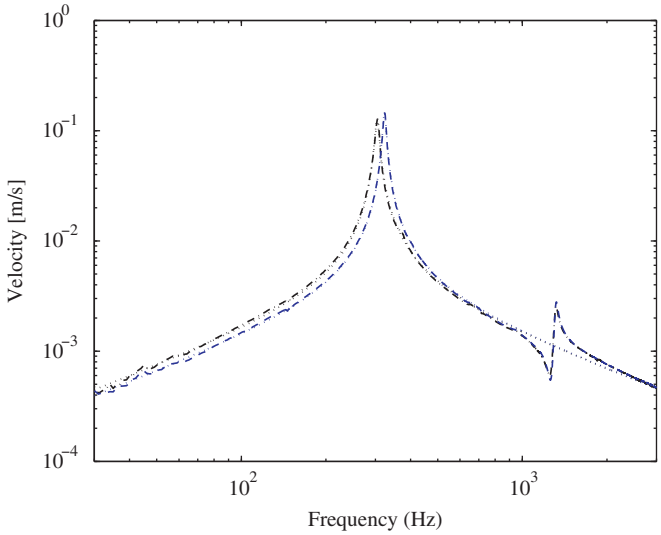

Fig. 6. Velocity responses of the inertial actuator for the ① short- (dash-dot line) and ② open-circuit (dashed) conditions whose natural frequencies are 304 and 323 Hz, respectively: experiments (dash-dot/dashed lines) and simulations (dotted). The parameters used for simulations are given in Table 3.

Table 3
Mechanical and electrical parameters of the plant (PCB 712A02) with a proof mass of 100 g.

m_s	f_s	f_{open}	ζ_s	C_p	σ	ϕ
117 g	304 Hz	323 Hz	0.018	69.8 nF	0.13	0.062 N/V

Effective structure mass m_s; short-circuit natural frequency f_s; open-circuit natural frequency f_{open}; short-circuit damping ratio ζ_s; capacitance of the piezoceramic actuator C_p; mass ratio σ; and EM conversion factor ϕ.

Nexus) for the accelerometer and a voltage amplifier (PCB 790A01) of fixed gain of 30 were also used as shown in Fig. 5. The discrete form for the control filter is given by [4,9]

$$H(z) = K_d \omega_a^2 \frac{T}{\omega_d} \frac{zA \sin \omega_d T}{z^2 - z(2A \cos \omega_d T) + A^2} \tag{26}$$

where $\omega_d = \omega_a \sqrt{1-\zeta_a^2}$, $A = \exp(-\zeta_a \omega_a T)$, and the sampling time is $T = 1/F_s$ with the sampling frequency $F_s = 30$ kHz. The mass ratio for the active EDA is determined by

$$\sigma = KT_{ae}T_{ef}/m_s, \tag{27}$$

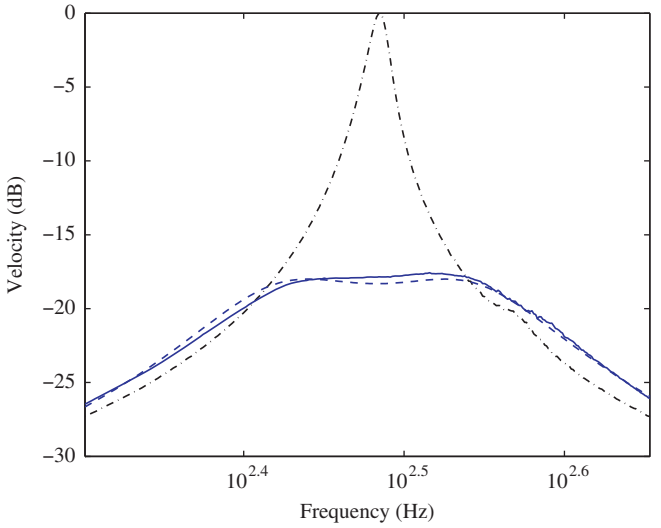

Fig. 7. Measured (solid line) and simulated (dashed) passive electrical dynamic absorber performances in terms of normalized velocities, compared with the original short-circuit plant response (measured, dash-dot) in Fig. 6, between 200 and 450 Hz.

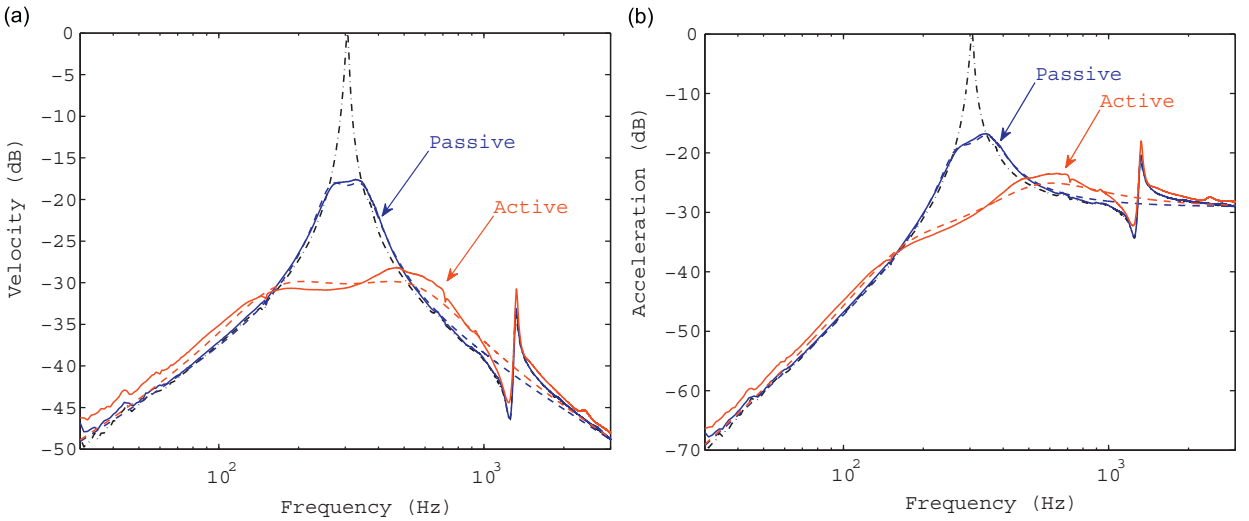

Fig. 8. Measured (solid line) and simulated (dashed) active electrical dynamic absorber performances in terms of normalized velocities (a) and accelerations (b), compared with the original short-circuit plant response (measured, dash-dot) in Fig. 6 and the passively controlled responses in Fig. 7.

where m_s is the structure mass, $K=K_dK_a$ in which the gains for the digital filter and the analog voltage amplifier were set to be $K_d=15$ and $K_a=30$, respectively, the transformation factor from acceleration to voltage in the signal conditioner was $T_{ae}=10$ mV/m s^{-2}, and the transformation factor from voltage to force in the inertial actuator (i.e., the EM conversion factor) was $T_{ef}=\phi=0.062$ N/V. The control algorithm used was again to achieve the maximally flat FRF using Eq. (22) that corresponds to the 2 dB (spillover) robust, optimal control strategy. The experimental (solid lines) and theoretical (dashed) velocity and acceleration responses after control are shown in Fig. 8(a) and (b), respectively, together with the corresponding original responses (dash-dot) in Fig. 6 and the corresponding passively controlled responses in Fig. 7 for comparison. There are slight differences between simulation and measurement because of the time delays due to the xPC target PC (53 μs=1.6/F_s) and the voltage amplifier (14 μs). Such time delays should be avoided as much as possible, for example, by employing an analog control filter as they reduce control performance and can threaten stability [4,10]. Fig. 8(b) clearly shows that the resonance due to the inertial actuator can be dramatically reduced by the passive and active methods. Some important features of the passive and active EDAs designed are summarized in Table 4. The optimal passive EDA gave a maximum vibration reduction of about 18 dB and a control bandwidth of 88 Hz (=351−263), while the active EDA with the gains ($K_d=15$ and $K_a=30$) gave about 30 dB reduction and a bandwidth of 344 Hz. In terms of the damping ratio, the original damping ratio of 1.8% turned to 25% by the passive method and turned to 109% by the active method. The

Table 4
Passive and active electrical dynamic absorbers designed.

Type	Mass ratio	Damping ratio	Max. reduction (dB)	Control bandwidth (Hz)
Passive	0.13	0.25	18	[263–351]
Active	2.39	1.09	30	[177–521]

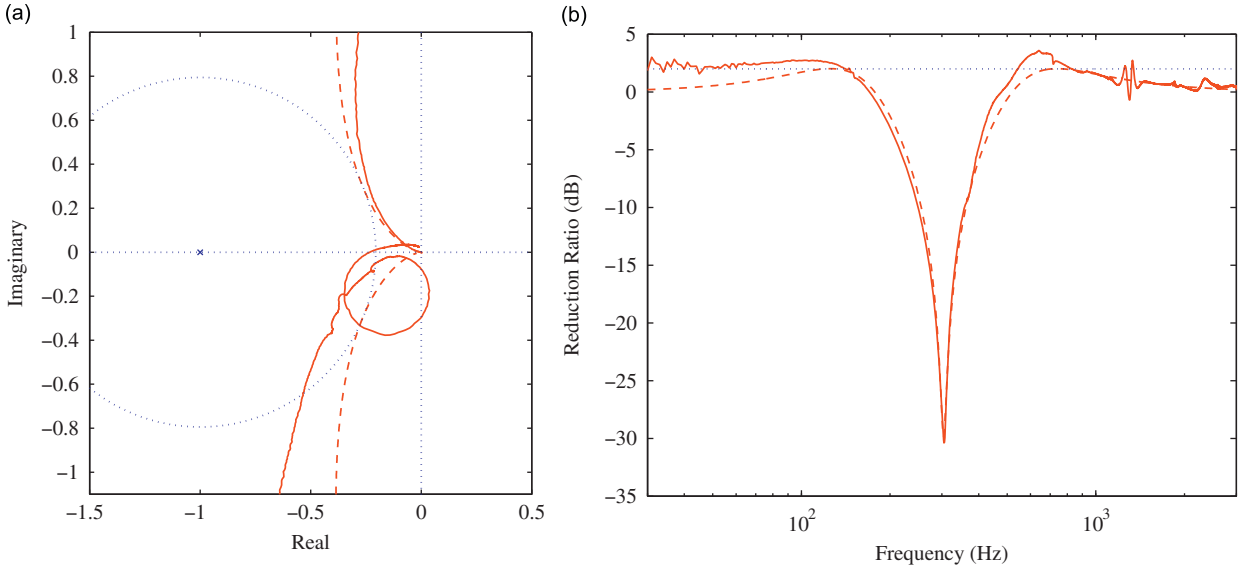

Fig. 9. Nyquist plots of the open-loop FRFs (a) and reduction ratios (b) of the active electrical dynamic absorber with measurement (solid line) and simulation (dashed), compared with the 2 dB robustness boundary (dotted).

control performances of the passive system were the maximum that could be achieved, whereas those for the active system could be improved upon. Unlike that for the passive method, note that the gain (K_d=15) used for the active system was arbitrarily chosen. It should be emphasized that the active EDA method employed is passivity-based control and thus it is, in principle, unconditionally stable.

To examine the robustness of the active system shown in Fig. 8, the open-loop FRFs (Nyquist plots) from simulation (dashed line) and measurement (solid) are plotted in Fig. 9(a), where the dotted circle around the instability point (-1, 0) indicates the 2 dB robustness boundary. The open-loop FRF was measured from the voltages between the xPC target controller (input) and the signal conditioner (output) in Fig. 5. The reduction ratios were also calculated by dividing the controlled response by the uncontrolled response, and are shown in Fig. 9(b), together with the 2 dB spillover line (dotted). The simulation locus almost exactly touches the 2 dB circle in Fig. 9(a) as was designed, supporting the optimization formulation developed. However, the measurement locus crosses the circle at high frequencies because of the time delays, as discussed earlier.

5. Concluding remarks

The dynamics of passive and active electrical dynamic absorbers (EDAs) have been analyzed using the impedance-mobility approach. The passive absorber was implemented by using an $R_s \| L_s$ parallel shunt circuit while the active absorber was implemented by feeding back the acceleration of the structure through a second-order lowpass filter. A simple but exact analogous model was presented, which was a *serially connected* mass–spring–damper oscillator. Such a mechanical analogy was possible, because of the introduction of the absorber damping ratio which is analogous to that for an $R_s \| L_s \| C_s$ parallel electric circuit. Using the impedance approach, it was demonstrated that the passive and active EDAs can be made exactly equivalent. Thus, the theoretical analysis framework and the analogous models developed are applicable to both types of EDAs. It should be emphasized that, although a SDOF vibration system has been examined, the theory is directly applicable to the coupling with a single vibration mode of a continuous system. It can be also extended to the coupling with multiple modes in a similar way conducted for vibroacoustic coupling [18].

The passive EDA was designed optimally by using Den Hartog's fixed-point theory with the aim to achieve a maximally flat coupled mobility FRF response of the structure (i.e., a maximally flat FRF strategy). The results state that the natural

frequency ω_a and the damping ratio ζ_a of the absorber must be

$$\omega_a = \omega_s \text{ and } \varsigma_a = \sqrt{\sigma/2},$$

where ω_s is the natural frequency of the host structure and $\sigma = m_{ca}/m_s$ is the mass ratio between the absorber m_{ca} and the structure m_s. The active EDA was designed using an optimal and robust control theory. By comparing the results from the two different methods for passive and active absorbers, it was concluded that the strategy for passive absorbers is compatible to the optimal, robust control of 2 dB control spillover. It should be noted that the analytical derivations became straightforward because of the introduction of the variable x, a normalized frequency bandwidth, for describing the related functions. Finally, simulations and experiments were conducted with a commercial inertial actuator that behaved as a single DOF oscillator, as the host structure to control. The results obtained clearly demonstrate good agreement between the theory and the experiments.

Appendix A. Two formulation methods for a piezoelectric shunt circuit

This appendix is a supplement to the impedance-mobility formulation in Section 2. Two formulation methods are compared, in common use for the dynamic equations of the piezoelectric shunt circuit shown in Fig. 1, with a particular emphasis on assigning signs: one based on the d_{33} piezoelectric effect and the other based on the d_{31} effect, where the first subscript denotes the poling direction and the second denotes the direction of motion of interest. The common sign conventions used are: (i) force and displacement are positive for tensions and expansions, respectively and (ii) voltage potential is assigned to be higher at the positively poled electrode.

The case based on the d_{33} effect is depicted in Fig. A1(a), where an external force is applied to a piezoceramic element. A negative voltage is then induced between the electrodes to resist the positive motion x, and the dynamic equation is given by

$$F_P = k_p x - \varphi V, \tag{A1}$$

where k_p is the stiffness of the short-circuited element and φ is an arbitrary electromechanical conversion factor that must be positive in this case. From Fig. A1(b), the charge q is related to motion and voltage as

$$q = \varphi x + C_p V, \tag{A2}$$

where C_p is the capacitance of the piezoceramic element. Eq. (A1) can be written as $x = (F_A + \varphi V)/k_p$. This and Eq. (A2) match with the general constitutive equations of piezoelectricity [8,19] with consistent signs (i.e., all positive). Since $I_L = -\dot{q}$ in Fig. A1(c) due to Kirchhoff's current law, $I_L = Z_L^{-1} V$ with Z_L being an arbitrary load impedance connected to the electrodes, and $v = \mathrm{d}x/\mathrm{d}t$, Eq. (A2) can be written as

$$-\varphi\, v = (j\omega C_p + Z_L^{-1})V. \tag{A3}$$

The formulation above can describe a d_{31} piezoelectric effect such as that shown in Fig. 1(a), if a negative value is allowed for φ, as in the standard [8].

Similarly, the case based on the d_{31} effect is illustrated in Fig. A2 in the same form as Fig. A1. The same procedure can be followed to give

$$F_P = k_p x + \phi V, \tag{A4}$$

$$q = -\phi x + C_p V, \tag{A5}$$

$$\phi v = (j\omega C_p + Z_L^{-1})V, \tag{A6}$$

where ϕ is the conversion factor for this case and is positive. Some authors use Eqs. (A1)–(A3) [3], and some others use Eqs. (A4)–(A6) including the authors of this paper [6,7]. The two sets equivalently represent a d_{31} piezoelectric effect when replacing $-\varphi$ by ϕ in Eqs. (A1)–(A3), or equivalently specifying a negative value for φ as in the standard [8]. Since this

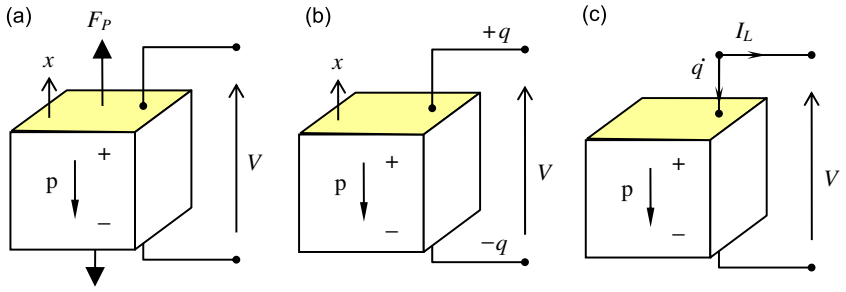

Fig. A1. Sign conventions of piezoelectricity using the d_{33} piezoelectric effect.

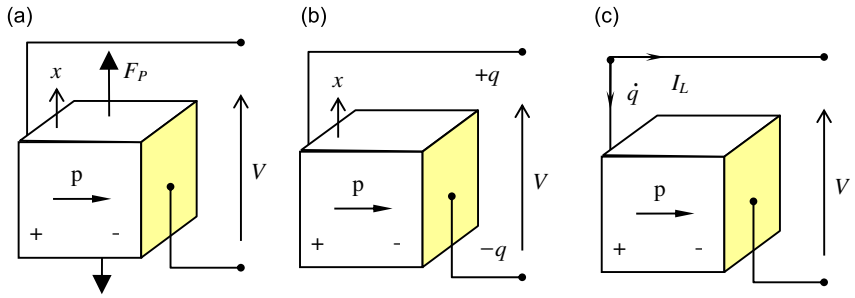

Fig. A2. Sign conventions of piezoelectricity using the d_{31} piezoelectric effect.

negative conversion factor in the first formulation is rather cumbersome in an intuitive sense for the purpose of this paper, however, the d_{31} case is used in this paper.

References

[1] N.W. Hagood, A. von Flotow, Damping of structural vibrations with piezoelectric materials and passive electrical networks, *Journal of Sound and Vibration* 146 (2) (1991) 243–268.
[2] G. Caruso, A critical analysis of electric shunt circuits employed in piezoelectric passive vibration damping, *Smart Materials and Structures* 10 (2001) 1059–1068.
[3] C.H. Park, Dynamics of beams with shunted piezoelectric elements, *Journal of Sound and Vibration* 268 (2003) 115–129.
[4] S.M. Kim, S. Pietrzko, M.J. Brennan, Active vibration isolation using an electrical damper or an electrical dynamic absorber, *IEEE Transactions on Control Systems Technology* 16 (2) (2008) 245–254.
[5] S.M. Kim, M.J. Brennan, A compact matrix formulation using the impedance and mobility approach for the analysis of structural acoustic systems, *Journal of Sound and Vibration* 223 (1999) 97–113.
[6] D. Guyomar, A. Badel, E. Lefeuvre, C. Richard, Toward energy harvesting using active materials and conversion improvement by nonlinear processing, *IEEE Transactions on Control Systems Technology* 52 (4) (2005) 584–595.
[7] Y.C. Shu, I.C. Lien, Analysis of power output for piezoelectric energy harvesting systems, *Smart Materials and Structures* 15 (2006) 1499–1512.
[8] *IEEE Standard on Piezoelectricity, IEEE Std.: 176-1978*, Institute of Electrical and Electronic Engineers Inc., New York, 1988.
[9] S.M. Kim, Active Control of Sound in Structural–acoustic Coupled Systems, PhD Thesis, University of Southampton, 1998.
[10] S.M. Kim, S.J. Elliott, M.J. Brennan, Decentralized control for multichannel active vibration isolation, *IEEE Transactions on Control Systems Technology* 9 (1) (2001) 93–100.
[11] S.B. Choi, H.S. Kim, J.S. Park, Multi-mode vibration reduction of a CD-ROM drive base using a piezoelectric shunt circuit, *Journal of Sound and Vibration* 300 (2007) 160–175.
[12] H.J. Sim, Structure-borne Noise Control of a Clamped Panel Using Piezoelectric Shunt Damping, PhD Thesis, Hanyang University, 2008.
[13] D.R. Cunningham, J.A. Stuller, *Circuit Analysis*, 2nd ed., John Wiley & Sons, Inc., 1995.
[14] J.P.Den Hartog, *Mechanical Vibration*, McGraw-Hill, New York, 1947.
[15] C.L. Davis, G.A. Lesieutre, An actively tuned solid-state vibration absorber using capacitive shunting of piezoelectric stiffness, *Journal of Sound and Vibration* 232 (3) (2000) 601–617.
[16] F.A.C. Viana, V. Steffen Jr., Multimodal vibration damping through piezoelectric patches and optimal resonant shunt circuits, *Journal of the Brazilian Society of Mechanical Sciences and Engineering* 29 (3) (2006) 293–310.
[17] A.J. Fleming, S. Behrens, S.O.R. Moheimani, Optimization and implementation of multimode piezoelectric shunt damping systems, *IEEE/ASME Transactions on Mechatronics* 7 (2002) 87–94.
[18] S.M. Kim, M.J. Brennan, Modeling a structural–acoustic coupled system with an equivalent lumped parameter mechanical system, *Journal of Vibration and Acoustics, Transactions of the ASME* 121 (1999) 453–459.
[19] A. Preumont, *Vibration Control of Active Structures: An Introduction*, Kluwer Academic Publishers, 1997.